Calculation and measurement of bianisotropy in a split ring resonator metamaterial

David R. Smith[a)]
Department of Electrical and Computer Engineering, Duke University, P.O. Box 90291, Durham, North Carolina 27708 and Department of Physics, University of California, San Diego, 9500 Gilman Drive, La Jolla, California 92093

Jonah Gollub
Department of Physics, University of California, San Diego, 9500 Gilman Drive, La Jolla, California 92093

Jack J. Mock
Department of Electrical and Computer Engineering, Duke University, P.O. Box 90291, Durham, North Carolina 27708

Willie J. Padilla
Los Alamos National Laboratory, MS K764, MST-10, Los Alamos, New Mexico 87545

David Schurig
Department of Electrical and Computer Engineering, Duke University, P.O. Box 90291, Durham, North Carolina 27708

(Received 2 June 2005; accepted 5 June 2006; published online 21 July 2006)

A medium that exhibits artificial magnetism can be formed by assembling an array of split ring resonators (SRRs)—planar conducting elements that exhibit a resonant response to electromagnetic radiation. The SRR exhibits a large magnetic dipole moment when excited by a magnetic field directed along its axis. However, the SRR also exhibits an electric response that can be quite large depending on the symmetry of the SRR and the orientation of the SRR with respect to the electric component of the field. So, while the SRR medium can be considered as having a predominantly magnetic response for certain orientations with respect to the incident wave, it is generally the case that the SRR exhibits magnetoelectric coupling, and hence a medium of SRRs arranged so as to break mirror symmetry about one of the axes will exhibit bianisotropy. We present here a method of directly calculating the magnetoelectric coupling terms using averages over the fields computed from full-wave finite-element based numerical simulations. We confirm the predicted bianisotropy of a fabricated SRR medium by measuring the cross polarization of a microwave beam transmitted through the sample. We also demonstrate that the magnetoelectric coupling that gives rise to the bianisotropic response is suppressed by symmetrizing the SRR composite structure and provide measurements comparing the cross polarization of the symmetric and asymmetric structures. [DOI: 10.1063/1.2218033]

I. INTRODUCTION

Since the demonstration of an artificially structured negative index medium[1]—one in which the electric permittivity and the magnetic permeability are both negative—there has been widespread interest in the properties of artificial media that derive their magnetic properties from periodically positioned conducting elements such as the split ring resonators (SRRs) shown in Fig. 1. The SRR medium was investigated theoretically by Pendry *et al.*,[2] who showed that SRRs possess a large magnetic polarizability. Because the resonance wavelength of the SRR can be much larger than its physical dimension, collections of SRRs can be used to form a composite medium characterized by a resonant effective permeability. Provided the overall material losses of the composite metamaterial are small enough, the effective permeability can be negative over a range of frequencies just above the resonance frequency. SRRs are therefore a convenient and frequency scalable means of obtaining negative permeability and have become a commonly used component in negative index and other metamaterials.[3–7] The artificial magnetic response of the SRR is particularly useful, since inherently magnetic materials are less available at higher frequencies and often require sizeable external static magnetic fields for bias.

While much of the interest in the SRR medium has developed in the context of negative index media, similar types of artificial media have been considered for many years in the context of chirality and bianisotropy.[8,9] While in the more recent work arrays of SRRs have been successfully utilized to form artificial magnetic media, the orientation of the SRR relative to the incident wave as well as the SRR design must be carefully controlled, otherwise, the electromagnetic response is significantly more complicated.

Consider the SRR unit cell shown in Fig. 1(a) [For convenience, we define a set of body axes that are fixed to the

[a)]Electronic mail: drsmith@ee.duke.edu

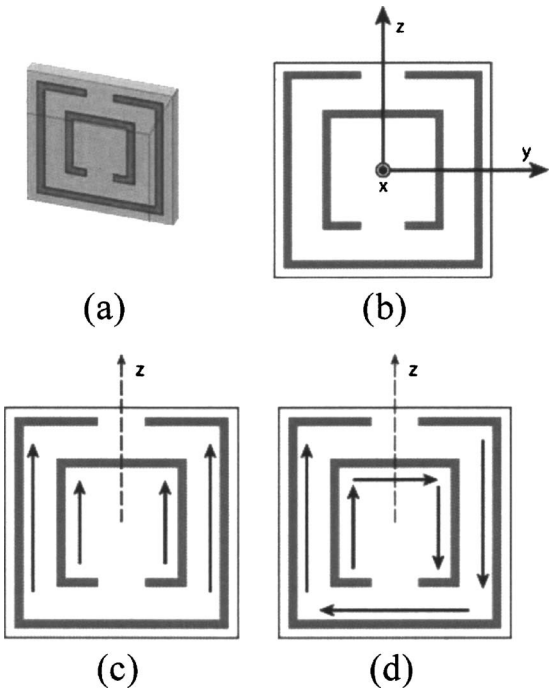

FIG. 1. (a) One unit cell of a SRR medium. This particular unit cell is used for the simulations and the measured structures presented later. The unit cell is cubic with lattice constant of 2.5 mm; the outer length of the outer ring is 2.1 mm; the linewidths are 0.13 mm; the gaps in the rings are 0.47 mm; the gap between inner and outer rings is 0.35 mm. The substrate thickness is 0.25 mm with a dielectric constant of 4.3. (b) The SRR shown with axes. (c) A schematic diagram of the currents associated with the SRR electric response. (d) A schematic diagram of the currents associated with the SRR magnetic or bianisotropic response.

SRR as indicated in Fig. 1(b), reorienting the axis of propagation depending on the SRR configuration.] The qualitative electromagnetic response of the SRR can be anticipated by considering various scenarios of the wave polarization relative to the SRR axes. An electric field directed along the z axis, for example, will induce an electric polarization in the SRR, since charge accumulates on opposite sides of the rings. The induced currents are indicated in Fig. 1(c). A time-alternating magnetic field directed along the x axis will generate a magnetic response, with circulating currents being induced in the rings, shown schematically in Fig. 1(d). Because the SRR contains capacitive gaps within and between the rings, the magnetic response of the SRR will be resonant, enabling the magnitude of the induced magnetic dipole to be quite large.

The lack of a mirror plane symmetry about the xy plane gives rise to an additional electromagnetic response. Under application of an electric field along the y direction, charging will be induced across the gaps in each ring of the SRR. Given the lack of an xy symmetry plane, the induced charge implies a net circulation of current. We thus see that, in general, the SRR exhibits a magnetoelectric coupled response, which cannot be encapsulated in a description involving only a permittivity and a permeability. Although this coupling can be easily removed by restoring symmetry to the medium—as we will show—it is of interest to characterize the basic bianisotropic response of the SRR medium design that has already been incorporated into many metamaterial designs. This study is also of interest as the magnetoelectric coupling has been used as a signature of magnetic activity in experiments on high frequency (e.g., terahertz and higher) planar SRR samples.[10,11]

To account for the magnetoelectric coupling in Maxwell's equations, we make use of the more general constitutive relationships,[12]

$$\mathbf{D} = \varepsilon_0 \varepsilon \mathbf{E} - i\sqrt{\varepsilon_0 \mu_0}\kappa \mathbf{H},$$
$$\mathbf{B} = i\sqrt{\varepsilon_0 \mu_0}\kappa^T \mathbf{E} + \mu_0 \mu \mathbf{H}. \tag{1}$$

An inspection of the anisotropic SRR unit cell in Fig. 1 suggests that only certain components of the permittivity, permeability, and magnetoelectric tensors are of significance, as has been noted by Marqués *et al.*;[13] specifically,

$$\varepsilon = \begin{bmatrix} 1 & 0 & 0 \\ 0 & \varepsilon_{yy} & 0 \\ 0 & 0 & \varepsilon_{zz} \end{bmatrix}, \quad \mu = \begin{bmatrix} \mu_{xx} & 0 & 0 \\ 0 & 1 & 0 \\ 0 & 0 & 1 \end{bmatrix}, \quad \kappa = \begin{bmatrix} 0 & 0 & 0 \\ \kappa_{yx} & 0 & 0 \\ 0 & 0 & 0 \end{bmatrix}. \tag{2}$$

We designate the nonzero components of the material parameter tensors with respect to the system of coordinates defined in Fig. 1(a) to maintain a description that is independent of the SRR orientation.

While a quantitative analytical analysis can be carried out to determine the relevant material parameters corresponding to a SRR medium, it is generally a difficult procedure and one that will rely on simplifying geometries.[14] Qualitatively, the material parameters have been shown to have the forms[13,14]

$$\varepsilon_{zz} = a,$$
$$\varepsilon_{yy} = a + \frac{b\omega^2}{(\omega_0^2 - \omega^2)},$$
$$\mu_{xx} = 1 + \frac{c\omega^2}{(\omega_0^2 - \omega^2)}, \tag{3}$$
$$\kappa_{yx} = \frac{d\omega_0\omega}{(\omega_0^2 - \omega^2)}$$

in the absence of losses. From Eqs. (3), we see that the component of permittivity in the direction of the ring gaps (z direction) should be frequency independent, although the mode indicated by Fig. 1(c) is actually resonant at much higher frequencies due to the capacitance between adjacent SRRs. Equations (3) also show that the component of permittivity along the axis that lies in the plane of the SRR but orthogonal to the gaps (y direction) should have a resonant form, along with the permeability component along the axis of the SRR (x direction) and the magnetoelectric component that relates the electric and magnetic responses along the y and x axes. The coefficients a, b, c, and d are related to the geometry of the SRR and any other materials that are placed in the unit cell. The resonant forms of Eq. (3), while not causal, nevertheless describe the medium response over the frequency range of interest. In a detailed numerical and ex-

perimental study on individual and small numbers of interacting SRRs, the general current distributions and corresponding scattering cross sections of the electric and magnetic modes have been identified and been shown to be consistent with magnetoelectric nature of the SRR resonance.[15]

II. SIMULATION OF MATERIAL PARAMETERS

To determine the electromagnetic material response from the output available from full-wave simulations, it is necessary to apply an appropriate algorithm to retrieve the "macroscopic" material parameters from the local field distributions, scattering parameters, or other computed quantities derived from the numerical solution of Maxwell's equations. The usefulness of this numerical retrieval procedure is that the detailed metamaterial physical structure—no matter how complicated or what materials are used—can be conceptually replaced by a homogeneous material whose electromagnetic characteristics are described by relatively few quantities.

A common method of parameter retrieval has been to compute first the scattering parameters (reflection and transmission coefficients) for one or more unit cells of a metamaterial structure and apply an inversion procedure to retrieve, for example, the relevant components of the permittivity and permeability.[16,17] In the absence of magnetoelectric coupling, this procedure can be readily applied, since computation of the complex reflection and transmission coefficients provides four computed or measured parameters that can be reexpressed in terms of the complex permittivity and permeability tensor elements appropriate for the given direction of propagation. When the magnetoelectric coupling term is also significant, however, more than one polarization and/or direction of incidence of the exciting wave must be applied, otherwise the number of unknown parameters exceeds the number of computed quantities. The development of a generalized *S*-parameters retrieval procedure has been initiated by Grzegorczyk *et al.*, who have demonstrated the feasibility of this approach in preliminary calculations on homogeneous bianisotropioc slabs.[18]

If our goal is the retrieval of the material parameters from simulated (not measured) structures, we can employ an alternative technique based on averaging the local fields computed in a full-wave simulation. We illustrate this approach here, using the SRR unit cell design illustrated in Fig. 1(a). The method of field averaging was suggested by Pendry *et al.* as an analytic tool to facilitate an effective medium description of the SRR and other artificial magnetic metamaterials.[21] Pendry *et al.* proposed that the local fields be averaged according to the following prescription:

$$\bar{E}_j = d^{-1}\int \mathbf{E}\cdot d\mathbf{x}_j, \quad \bar{D}_j = d^{-2}\int \varepsilon_{\mathrm{loc}}(\mathbf{x})\mathbf{E}\cdot d\mathbf{s}_j,$$
$$\bar{H}_j = d^{-1}\int \frac{\mathbf{B}}{\mu_{\mathrm{loc}}(\mathbf{x})}\cdot d\mathbf{x}_j, \quad \bar{B}_j = d^{-2}\int \mathbf{B}\cdot d\mathbf{s}_j, \tag{4}$$

where $\varepsilon_{\mathrm{loc}}(\mathbf{x})$ and $\mu_{\mathrm{loc}}(\mathbf{x})$ are the local permittivity and permeability functions that vary spatially throughout the unit cell, and d is the side length of the cubic unit cell. In Eq. (4) and throughout the remainder of this paper, we work with the actual rather than the relative permittivity and permeability tensors, thus removing the explicit appearance of ε_0 and μ_0. Equations (4) show that the macroscopic field components $\bar{E}$ and $\bar{H}$ can be found from line integrals over the local fields, while the macroscopic field components $\bar{D}$ and $\bar{B}$ can be found from surface integrals of the local fields taken over any of the faces of the unit cell. In the absence of magnetoelectric coupling, the components of the permittivity and permeability tensors can be found by taking the appropriate quotients of the averaged fields, that is,

$$\varepsilon_j \equiv \bar{D}_j/\bar{E}_j, \quad \mu_j \equiv \bar{B}_j/\bar{H}_j. \tag{5}$$

While Eqs. (4) are strictly valid in the static limit, it was shown by an empirical argument that with a minor modification, Eqs. (4) could be extended to all frequencies of interest.[19] The field averaging method is thus a viable alternative to *S*-parameters retrieval for the determination of the material parameters for simulated structures. A rigorous justification of Eqs. (4) has recently been presented;[20] both the field averaging method and *S*-parameters retrieval have been shown to produce identical results for simulated nonbianisotropic metamaterials.

For the numerical simulations presented here, we make use of the eigensolver module in HFSS (Ansoft). HFSS is a commercial, finite-element based electromagnetic mode solver. In the eigensolver module, the electromagnetic fields are computed within a single unit cell (in this case cubic), with either periodic boundary conditions or combinations of perfect electric and magnetic boundary conditions applied to the bounding surfaces to model the infinite structure. To simulate the propagation of a plane wave through the artificial medium, we apply periodic boundary conditions with a specified phase advance along one of the axes—the propagation direction—with periodic, electric, or magnetic boundary conditions assigned to the bounding surfaces normal to the remaining two axes.

Four possible orientations of the SRR relative to the polarization and propagation directions of the incident wave are shown in Fig. 2. In orientation (A), the SRR responds with a predominantly magnetic resonant response to the propagating electromagnetic field. Note that since there is no symmetry plane normal to the z axis, magnetoelectric coupling is present and produces a field component in the direction of propagation. Because the divergence of the macroscopic displacement field is zero, $D_y=0$ and we find from Eqs. (1),

$$D_z = \varepsilon_{zz}E_z,$$
$$B_x = \left(\mu_{xx} - \frac{\kappa_{yx}^2}{\varepsilon_{yy}}\right)H_x. \tag{6}$$

The magnetoelectric coupling in this case does not cross couple the transverse magnetic and electric fields, although the average of B_x/H_x does not correspond to μ_{xx}. Although we find in practice that the ratio of the field averages B_x/H_x corresponds reasonably well with the predicted form for the permeability μ_{xx}, nevertheless, Eqs. (6) show that it is only an approximate relationship at best. Similarly, the SRR in

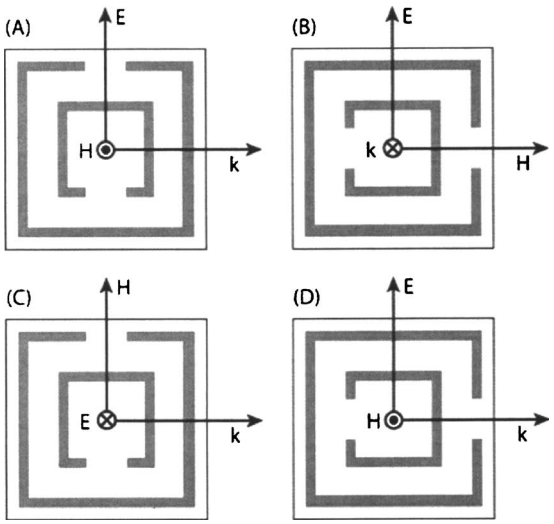

FIG. 2. Four possible orientations of the SRR relative to the propagation direction and polarization of the incident wave.

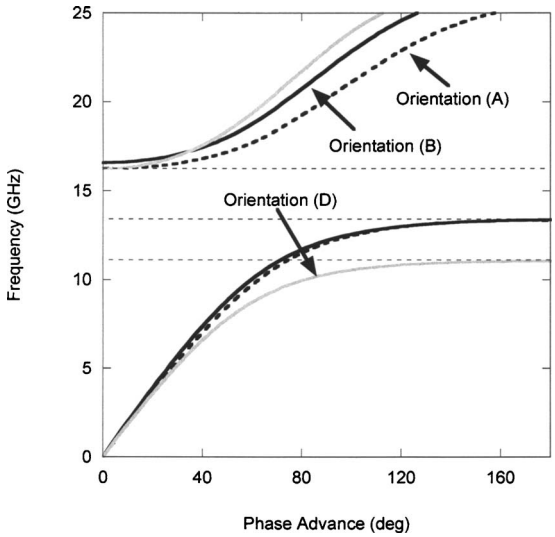

FIG. 3. Computed dispersion curves for the SRR medium, with the SRRs oriented for predominantly magnetic response (dashed black curve), electric response (solid black curve), and magnetoelectric response (solid gray curve).

orientation (B) responds with a predominantly electric resonant response, with the magnetoelectric coupling producing a magnetic response in the direction of propagation. Constitutive relationships similar to those in Eqs. (6) can be found for this orientation as well.

In orientation (D), the SRR responds with resonant electric $\varepsilon_{yy}(\omega)$, magnetic $\mu_{xx}(\omega)$, and magnetoelectric $\kappa_{yx}(\omega)$ responses. In this case, because all responses are in the transverse directions, the magnetoelectric coupling cannot be ignored and influences the propagation characteristics of the wave. Finally, in orientation (C) the SRR exhibits negligible electromagnetic response.

The analysis of orientation (D) by field averaging is complicated by the magnetoelectric coupling. Keeping only the nonnegligible terms in Eqs. (1), and bearing in mind that the direction of wave propagation is now along the z axis, we have

$$D_y = \varepsilon_{yy} E_y - i\kappa_{yx} H_x,$$
$$B_x = i\kappa_{yx} E_y + \mu_{xx} H_x. \tag{7}$$

In general, Eqs. (7) are insufficient to allow the determination of the material parameters, as there are two equations and three unknowns. The dispersion relation, which is computed naturally in the eigensolver, can be used to provide the additional needed information. As shown by Marqués *et al.*,[13] if the constitutive relations in Eqs. (7) are used with Maxwell's equations, plane wave solutions are found with wave vector,

$$k_y = \sqrt{\varepsilon_{yy}\mu_{xx} - \kappa_{yx}^2}\,\frac{\omega}{c}, \tag{8}$$

where ω is the angular frequency, c is the speed of light in vacuum, and k_y is the wave number in the direction relative to the SRR as shown in Fig. 2(d).

Equations (7) and (8) should provide a complete description of the material parameters corresponding to the SRR medium. Indeed, an expression relating κ_{xy} to the obtainable field averages has been recently been presented.[20] However, because we are utilizing the eigensolver as our method of simulation, there are some limitations that arise specific to this simulation technique. For example, we are unable to compute the modes—and hence the fields—for frequencies that are forbidden. For cases where no magnetoelectric coupling is present, forbidden frequencies occur where either ε or μ (but not both) are less than zero. By contrast, for configuration (D), Eq. (8) shows that the forbidden region will be larger, as has been pointed out previously.[13] The dispersion curves computed for SRR unit cell, presented in Fig. 3, confirm this: the frequency band gap is larger for orientation (D) than for either orientation (A) or (B). To overcome some of the limitations of the eigensolver method, other simulation techniques, such as driven frequency- or time-domain methods, could be used with the field averaging approach to retrieve material parameters over all frequencies.

A second limitation that may arise with the eigensolver method is that lossy materials are not traditionally implemented. While HFSS has a solver that can produce the complex eigenfrequencies and eigenmodes of a lossy structure, a significant reduction in complexity is achieved if we simulate lossless materials. In this case, we may assume ε_{yy}, μ_{xx}, and κ_{yx} are all real functions of frequency, and we find from Eqs. (7),

$$\kappa_{xy} = -\frac{\mathrm{Im}(D_y/E_y)}{\mathrm{Re}(1/z)},$$
$$\kappa_{xy} = \frac{\mathrm{Im}(B_x/H_x)}{\mathrm{Re}\, z}, \tag{9}$$

and from Eq.(8),

$$\varepsilon_{yy} = \mathrm{Re}\left(\frac{D_y}{E_y}\right) - \kappa_{xy}\,\mathrm{Im}\left(\frac{1}{z}\right), \tag{10}$$

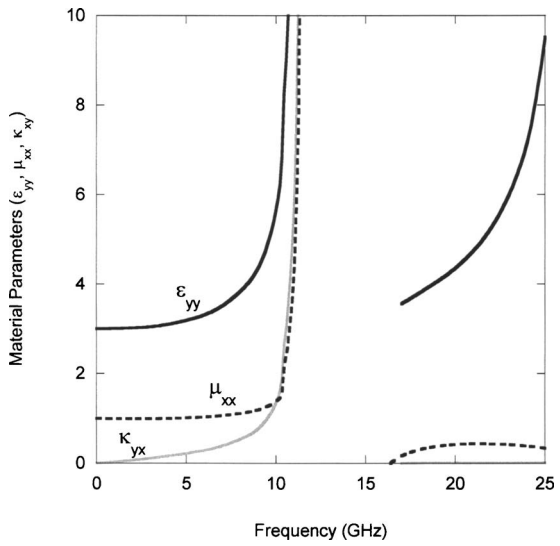

FIG. 4. The material parameters as computed by averaging the local fields of the simulated modes.

$$\mu_{xx} = \mathrm{Re}\left(\frac{B_x}{H_x}\right) + \kappa_{xy}\,\mathrm{Im}(z),$$

where z is the ratio E_y/H_x. Equations (9) and (10) enable us to completely characterize the effective medium parameters of the lossless bianisotropic SRR medium without the use of the dispersion relation [Eq. (8)]. The additional information provided by Eq. (8) is redundant for a lossless structure, and can be used as a means of verifying the consistency of the computed effective medium parameters.

The averaging method was tested on the SRR unit cell shown in Fig. 1, in which the geometrical parameters for this metamaterial are summarized. The effective medium material parameters computed by the procedure outlined in Eqs. (9) and (10) are presented in Fig. 4. As revealed by the dispersion curves in Fig. 3, there is a forbidden frequency gap predicted between 11.1 and 16.2 GHz. Below this gap, the retrieved parameters are in qualitative agreement with Eqs. (3). Above the gap region, there is a departure of the simulated functions from the ideal functions. This difference is due to the spatial dispersion and higher order band effects inherent to the periodic structure of the actual metamaterial. The effects due to spatial periodicity are not predicted by the analytical model that leads to Eqs. (3). Note from Fig. 4 that while this particular SRR design results in a resonant permeability, the resonance of the permittivity is actually significantly larger in magnitude. It is often the case in SRR media—and appears to be even more prevalent in higher frequency designs such as those recently reported[11]—that the electric response dominates the magnetic response. It is not immediately clear why this should be the case, but it should be noted that the permittivity actually includes the effects of two electric resonances. One of the resonances is due to the bianisotropic modes with circulating currents, the other is due to the excitation of linear currents [see Figs. 1(b) and 1(c)]. The latter mode produces a strong dc and low frequency electric response that dominates the magnetic response. The frequency separation and relative oscillator strengths of the two modes will strongly impact the observed permittivity and its relative magnitude versus that of the permeability.

The boundary conditions applied in the propagation direction (z direction) for orientation (D) imply that the simulated structure is asymmetric—that is, has a lack of mirror plane symmetry about one axis. We can alternatively simulate the symmetric structure by appropriate choice of boundary conditions. For example, for the SRR in orientation (A), a choice of perfect electric conducting boundary conditions in the z direction leads to a symmetrized structure for waves propagating in the y direction. Likewise, for the SRR in orientation (B), a choice of perfect magnetic conducting boundary conditions in the z direction leads to a symmetrized structure for waves propagating in the x direction. In either case, the infinitely repeated structure is symmetric, with all axes possessing mirror symmetry. As a control, the unit cell simulations were repeated using these boundary conditions. Although a 2 GHz shift in frequency occurred, the recovered permittivity and permeability for the symmetric structure were qualitatively as in Fig. 4 for the asymmetric structure. The magnetoelectric coupling term, however, was many orders of magnitude lower than that found for the asymmetric structure—essentially within the computational noise floor—as would be expected.

As described above [see Eq. (8)], the off-diagonal terms of the magnetoelectric tensor κ lead to plane wave eigensolutions of Maxwell's equations for propagation along any of the principal axes. That is, there is no cross polarization as long as the wave propagates through the medium along a principal axis. This is not true, however, for waves of arbitrary incidence, so that the off-diagonal magnetoelectric coupling term will generally lead to a more complicated polarization state for waves propagating along a direction for which the diagonal elements κ are nonzero. In what follows, we use this polarization conversion as a means to confirm the computed values of κ_{yx}.

III. EXPERIMENTAL CHARACTERIZATION OF SRRS

Various SRR medium samples were assembled from fabricated strips of SRRs having the dimensions described in Fig. 1. This particular SRR design has been used previously to demonstrate the existence of magnetic surface plasmons and is summarized in more detail elsewhere.[21] The SRRs were designed so that their resonance occurred over a band of microwave frequencies consistent with our network analyzer (Agilent N5230A PNA-L) and other measurement equipment. The SRRs were fabricated using standard optical lithography. Photosensitized half-ounce copper-clad FR-4 circuit board formed the substrate material ($\sim$17 μm copper thickness). A mask was designed consisting of strips of 2.5 mm SRR unit cells extending 6 cells wide and 70 cells long (15×175 mm^2); the mask was printed on a transparency having a resolution of 1200 dots/in. The photosensitized copper clad FR-4 was covered by the mask and exposed to ultraviolet light for 5 min in a Kinsten three-bulb UV exposure unit. The photoresist was developed in a sodium carbonate solution and then placed in an etching solu-

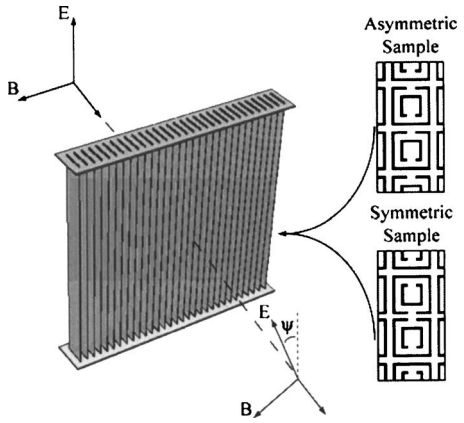

FIG. 5. Schematic diagram of the 0° SRR medium sample.

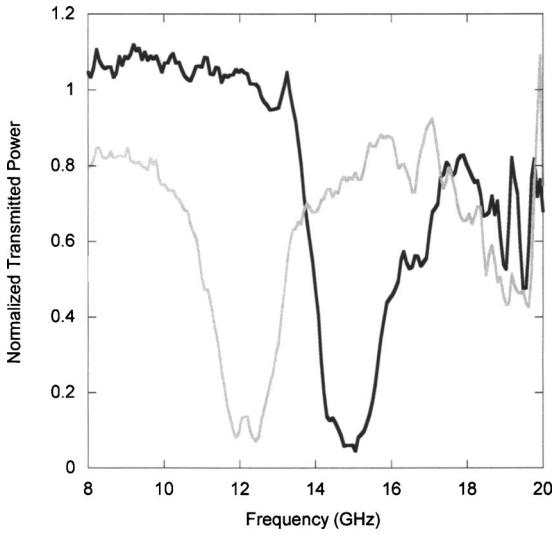

FIG. 6. Transmitted power through the 0° SRR medium sample, for asymmetric SRRs (black curve) and symmetric SRRs (gray curve).

tion (ferric chloride) for 15 min during which its orientation was inverted once to ensure even etching. Finally, the board was placed in a stripper solution (potassium hydroxide) for 10 min to remove the remaining photoresist. The strips of SRRs were cut out, each being 1.5 cm (6 unit cells) in width and 15 cm (60 unit cells) in height. Supporting cross strips, constructed from bare FR-4 substrate material, were used to assemble the strips into three-dimensional (3D) slabs as shown in Figs. 5 and 7. Two sets of support strips were fabricated such that the SRR strips could be assembled either at 0° or 45° with respect to the wave vector of the incident radiation. The assembled samples had final dimensions of $150\times150\times15$ mm^3.

The SRRs were first assembled into an orthogonal slab sample, as depicted in Fig. 5, with the split ring unit cells oriented "asymmetrically." Waves were normally incident on the assembled slab, propagating relative to the SRRs as illustrated in Fig. 2(a). For this orientation, a magnetic response is expected to dominate the electromagnetic properties. As has been well established in previous experiments, where the resonant permeability takes values less than zero a forbidden band gap occurs, manifesting as a region of attenuation in transmission measurements. From the computed dispersion curve in Fig. 3, we expect the frequency band gap to be between 13.2 and 16.2 GHz.

Transmission measurements were performed with the sample suspended 2 ft above an optical table through a 6 in. square by $\frac{1}{2}$ in. thick aperture. Source and detector standard gain X-band horns (Advanced Technical Materials 8.2–12.4 GHz) were placed facing each other at 4 ft separation with the sample in the middle. The horns were elevated relative to the table at the same height as the sample. Measurements were then made of the sample using the network analyzer normalized to the empty aperture. The transmission data shown in Fig. 6 (black curve) reveal a region of attenuation consistent with the predicted band gap.

A second orthogonally oriented sample was fabricated, using the same method as described above, except the SRR in each successive cell was rotated (in plane) 180° relative to its neighbor, as depicted in the inset to Fig. 5. These rotations symmetrized the structure, adding an xy mirror plane and doubling the unit cell. Simulations that use electric or magnetic boundary conditions instead of periodic boundary conditions describe this type of symmetrized structure. Since the symmetric sample consists of a bipartite lattice of both orientations of SRRs, the polarization mixing that happens from one orientation is "unmixed" by averaging with the other orientation in a neighboring unit cell. The resonance of the symmetric sample, however, is detuned relative to that of the asymmetric sample. As can be seen from Fig. 6, the region of negative permeability of the symmetric sample lies roughly 2.5 GHz lower than that of the asymmetric sample.

As described in Sec. I, when a wave is incident along a direction other than one of the principal axes, the possibility exists for cross polarization. For example, if we start with the direction of incidence indicated in Fig. 2(a), where the only nonzero component of $\boldsymbol{\kappa}$ is κ_{yx}, and rotate the coordinate system by an angle θ in the xy plane, we find

$$\boldsymbol{\kappa}' = \begin{pmatrix} -\kappa_{yx}\cos\theta\sin\theta & -\kappa_{yx}\sin^2\theta & 0 \\ \kappa_{yx}\cos^2\theta & \kappa_{yx}\cos\theta\sin\theta & 0 \\ 0 & 0 & 1 \end{pmatrix}. \tag{11}$$

Since the degree of cross polarization is roughly proportional to the magnitude of the diagonal elements in the $\boldsymbol{\kappa}$ tensor, we expect the maximum amount of cross polarization when the SRRs are rotated in the xy plane by 45°.

To characterize the magnetoelectric coupling term, we formed a second sample using the same SRR strips, but configured as depicted in Fig. 7, where the individual slabs are placed in the sample at 45° with respect to the wave vector of the incident field. Once again, symmetric and asymmetric versions of the sample were assembled so as to compare the degree of cross polarization. The strips in these 45° samples were assembled such that the incident wave made a 45° angle from the principal axis direction of Fig. 2(a). This orientation was chosen to maximize the expected cross polarization.

Measurements on the various samples are presented in Fig. 8. The power transmitted with no sample present, shown as the solid gray curve, provides a base line normalization to which the subsequent data can be compared. Because the

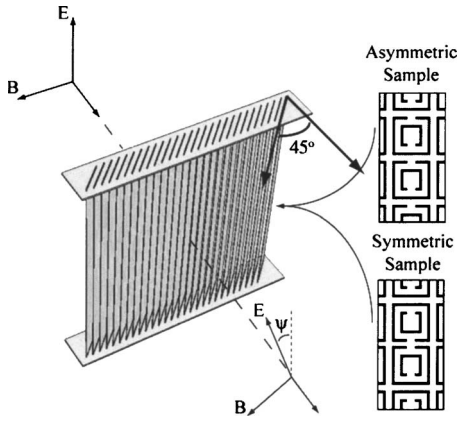

FIG. 7. Schematic of the 45° SRR medium sample.

broadband horns used in the experiment are fed by X-band waveguide (8.2–12.4 GHz), the valid range of measurement is much narrower than the range shown in the figure. On the low frequency end the transmitted power is abruptly attenuated due to the waveguide cutoff, while the transmitted power also rolls off on the high frequency end where higher order modes are presumably excited in the waveguide feed. Depending on the information of interest, however, the horns can be utilized somewhat outside their optimal range, so we present the data over the broader frequency range (5–20 GHz).

For the measurement of cross polarization, the broadband horns were configured for direct transmission, such that the *E* plane of one horn was oriented 90° with respect to the other horn. With no sample present, the cross-polarized transmitted power measured (dashed gray curve in Fig. 8) was −35 dB down from the parallel-polarized transmitted power. The 0° slab sample exhibited a level of cross polarization roughly commensurate with that of no sample

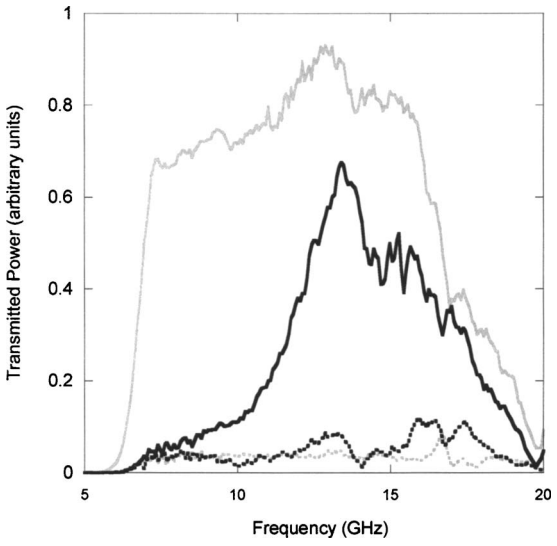

FIG. 8. Comparison of cross-polarization measurements for the asymmetric 0° SRR medium (black dashed curve) and the asymmetric 45° SRR medium (solid black curve). For calibration, measurements of the transmission with horns aligned (solid gray curve) and cross polarization (dashed gray curve) are shown for no sample present. The shape of the solid gray curve is set by the characteristics of the standard gain X-band microwave horn used in the experiments.

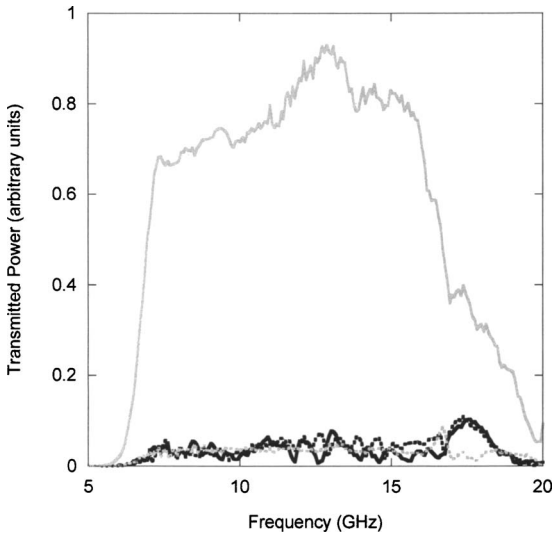

FIG. 9. Comparison of cross-polarization measurements for the symmetric 0° SRR medium (black dashed curve) and the symmetric 45° SRR medium (solid black curve). The transmission (solid gray curve) is shown again for no sample present, horns aligned. The dashed gray line corresponds to the asymmetric 45° SRR medium with alternating planes.

present, as expected. The 45° sample, however, exhibited a strong cross-polarized transmittance which, as a function of frequency, appears to be qualitatively consistent with the resonant form for κ predicted by Eqs. (2). Using the transmitted power with no sample present as a normalization, we see that at resonance nearly 80% of the power transmitted is cross polarized.

For comparison, the same data set was taken on a 45° SRR medium sample, in which the SRR strips were symmetrically oriented (e.g., see Fig. 7). Figure 9 shows that no evidence of cross-polarization transmission was present for the symmetric sample, as would be expected from symmetry arguments. A second 45° sample was formed using the asymmetric SRR strips, but this time alternating the orientation of each subsequent strip such that the gaps in the SRRs were opposite on successive strips. As shown by the dashed gray curve in Fig. 9, the alternating layer structure also exhibits little or no cross polarization, indicating that the magnetoelectric coupling has been approximately canceled.

IV. COMPARISON WITH TRANSMISSION MODEL

While the measured cross polarization in Fig. 8 appears qualitatively to track the expected resonant form of the magnetoelectric term (in magnitude) as a function of frequency, it does not provide for a quantitative comparison. To make the comparison quantitative, it is necessary to calculate the magnitude of the cross polarization of a wave transmitted through a homogeneous planar slab with the constitutive relations as in Eqs. (1), with parameters determined from the finite-element field-averaging calculations (Fig. 4). Comparison of the measured and computed cross polarization provides a means of quantifying the magnetoelectric coupling term.

A method of calculating the transmission characteristics of a multilayer stack of bianisotropic materials has been described by Grzegorczyk *et al.*,[18] which we summarize briefly

here. The transmission calculation can be cast as an eigenvector/boundary value problem. Assuming an $e^{-i\omega t}$ dependence for the fields, an application of Maxwell's equations provides an eigenvalue equation in terms of the parallel field components,

$$\frac{\partial}{\partial z}\begin{pmatrix}\mathbf{E}_{\parallel}\\ \mathbf{B}_{\parallel}\end{pmatrix} = \mathbf{M}_j\begin{pmatrix}\mathbf{E}_{\parallel}\\ \mathbf{B}_{\parallel}\end{pmatrix}. \tag{12}$$

where $\mathbf{M}_j$ is a (6×6) matrix that represents the bianisotropic coupling between the fields and the index j identifies the material (free space or the SRR structure). Equation (12) can be solved to find a set of polarization states (the eigenvectors), defined by the matrix, $\boldsymbol{\nu}_j$, and an associated set of wavevectors (the eigenvalues), defined by the diagonal matrix $\boldsymbol{\beta}_j$. The fields can then be written in terms of these polarization states,

$$\begin{pmatrix}\mathbf{E}_{\parallel}\\ \mathbf{B}_{\parallel}\end{pmatrix} = \mathbf{v}_j \cdot e^{i(\boldsymbol{\beta}_j\cdot\hat{z})z}\cdot \mathbf{A}_j, \tag{13}$$

where $\mathbf{A}_j$ is vector containing the coefficients of each polarization state. Since parallel field components must be continuous across a boundary, we can use Eq. (13) to write a set of boundary value equations. With the two resulting equations at the front and back surfaces of the SRR structure and knowledge of the initial polarization state, we can solve for the cross-polarization coefficient of the transmitted radiation.

A program was written using MATLAB to implement Eqs. (12) and (13). The transmission calculations confirmed that for the material parameters corresponding to the asymmetric 0° sample, the incident radiation remains linearly polarized as it passes through the SRR structure. For the 45° asymmetric sample, however, the incident radiation couples to generally complicated eigenvector states that rotate and shift the phase of the fields. As a result, the radiation transmitted through the 45° sample becomes elliptically polarized.[22] As the slab thickness increases, more power is expected to be observed in the cross-polarized direction.

The computed cross polarization is compared with measurements in Fig. 10. Because we are unable to compute modes within the frequency band gap, and because the high frequency side of the resonance occurs where the X-band horns are multimode, the only reasonable band of frequencies for comparison occurs on the low frequency side of the resonance. The computed cross polarization, the gray curve in Fig. 10, is in reasonable agreement in trend and magnitude with the measured data. The measured cross-polarized transmitted power was normalized to the transmitted power with horns aligned (gray curve in Fig. 8), so that a quantitative comparison could be made with the transmission calculation.

V. CONCLUSION

Although SRRs have been utilized for their magnetic properties over the last several years, they in fact have a complicated, coupled electromagnetic response that is predominately magnetic only under certain restrictive conditions. Consistent with these restrictions, SRRs have been utilized to form negative index composites and to demonstrate specific phenomena. In these experiments, the direction and polarization of the incident wave have been chosen to avoid the more complicated electromagnetic effects. However, as shown by the simulations and measurements presented above, the magnetoelectric coupling is a relatively large effect in (asymmetric) SRR composites; for applications in which wave propagation will occur along arbitrary directions relative to the principal axes (lenses, for example) unwanted cross polarization can occur.

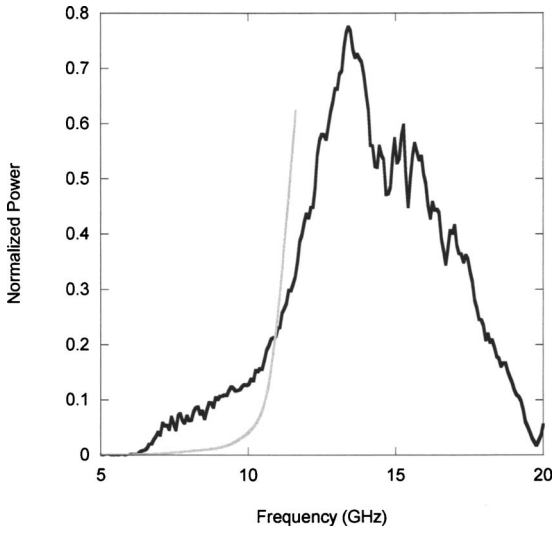

FIG. 10. Comparison of predicted cross polarization with the measured data, asymmetric 45° sample. Both the measured data and calculated curve are normalized such that a value of 1 indicates 100% cross polarization.

It is clear that the cross-polarization effects can be minimized by making the unit cell or a larger "supercell" of the metamaterial structure symmetric. In cases where bianisotropy is a desired property, however, we have presented an alternative means of computing and characterizing the relevant material parameters.

ACKNOWLEDGMENTS

This work was supported by DARPA (Contract No. MDA972-01-2-0016). In addition, one of the authors (D.S.) acknowledges support from the Director of Central Intelligence (DCI) Postdoctoral Research Fellowship Program, and another author (W.J.P.) acknowledges support from the Los Alamos National Laboratory LDRD Director's Fellowship. The authors are grateful to Dr. R. Marques and J. Baena for providing analytical results for comparison of the simulation data, and to Dr. Tomasz Grzegorczyk for extensive comments and discussion.

[1] D. R. Smith, W. J. Padilla, D. C. Vier, S. C. Nemat-Nasser, and S. Schultz, Phys. Rev. Lett. **84**, 4184 (2000).
[2] J. B. Pendry, A. J. Holden, D. J. Robbins, and W. J. Stewart, IEEE Trans. Microwave Theory Tech. **47**, 2075 (1999).
[3] A. A. Houck, J. B. Brock, and I. L. Chuang, Phys. Rev. Lett. **90**, 137401 (2003).
[4] C. G. Parazzoli, R. B. Greegor, K. Li, B. E. C. Koltenbah, and M. Tanielian, Phys. Rev. Lett. **90**, 107401 (2003).
[5] C. G. Parazzoli, R. B. Greegor, J. A. Nielsen, M. A. Thompson, K. Li, A. M. Vetter, M. H. Tanielian, and D. C. Vier, Appl. Phys. Lett. **84**, 3232 (2004).
[6] R. W. Ziolkowski, IEEE Trans. Antennas Propag. **51**, 1516 (2003).
[7] T. J. Yen, W. J. Padilla, N. Fang, D. C. Vier, D. R. Smith, J. B. Pendry, D.

N. Basov, and X. Zhang, Science **303**, 1494 (2004).
[8]M. M. I. Saadoun and N. Engheta, Microwave Opt. Technol. Lett. **5**, 184 (1992).
[9]W. S. Weiglhofer, Int. J. Appl. Electromagn. Mech. **9**, 93 (1998).
[10]T. Koschny, M. Kafesaki, E. N. Economou, and C. M. Soukoulis, Phys. Rev. Lett. **93**, 107402 (2004).
[11]S. Linden, C. Enkrich, M. Wegener, J. F. Zhou, T. Koschny, and C. M. Soukoulis, Science **306**, 1351 (2004).
[12]J. A. Kong, *Electromagnetic Wave Theory*, 2nd ed. (Wiley, New York, 1990), Sec. 2.6.
[13]R. Marqués, F. Medina, and R. Rafi-El-Idrissi, Phys. Rev. B **65**, 144440 (2002).
[14]R. Marqués, F. Mesa, J. Martel, and F. Medina, IEEE Trans. Antennas Propag. **51**, 2572 (2003).
[15]P. Gay-Balmaz and O. J. F. Martin, J. Appl. Phys. **92**, 2929 (2002).
[16]D. R. Smith, S. Schultz, P. Markos, and C. M. Soukoulis, Phys. Rev. B **65**, 195104 (2002).
[17]X. D. Chen, T. M. Grzegorczyk, B.-I. Wu, J. Pacheco, and J. A. Kong, Phys. Rev. E **70**, 016608 (2004).
[18]T. M. Grzegorczyk, X. Chen, J. Pacheco, J. Chen, B.-I. Wu, and J. A. Kong, Electromagn. Waves. **51**, 83 (2005).
[19]D. R. Smith, D. C. Vier, N. Kroll, and S. Schultz, Appl. Phys. Lett. **77**, 2246 (2000).
[20]D. R. Smith and J. B. Pendry, J. Opt. Soc. Am. B **23**, 391 (2006).
[21]J. N. Gollub, D. R. Smith, D. C. Vier, T. Perram, and J. J. Mock, Phys. Rev. B **71**, 195402 (2005).
[22]J. D. Jackson, *Classical Electrodynamics*, 3rd ed. (Wiley, New York, 1998).